



Effective adsorption of antimony(III) by MIL-101(Cr)-NH₂: influencing-factor and characterization analyses and response surface optimization

Tian Tian^a, Yannan Jia^{b,c}, Jianguo Wu^d, Jinlong Zhao^d, Kai Xu^a, Zijie Wang^e, Zheng Wang^{a,*}

^aSchool of Civil Engineering, Nanjing Forestry University, Longpan Road 159#, Nanjing 210037, China, Tel. +86 25 85427691; emails: wangzheng@njfu.edu.cn (Z. Wang), Tiantian@njfu.edu.cn (T. Tian), horizonxk@163.com (K. Xu)

^bState Key Laboratory of Simulation and Regulation of Water Cycle in River Basin, China Institute of Water Resources and Hydropower Research, Beijing 100038, China, email: jiayn@iwhr.com

^cChina Institute of Water Resources and Hydropower Research, Beijing 100038, China

^dHuaneng Weihai Power Generation Co., Ltd., Weihai 264205, China, emails: wjg_1617@163.com (J. Wu), Z13863103232@163.com (J. Zhao)

^eSchool of Architectural Engineering, Maanshan University, Maanshan 243100, China, email: wzj854333843@163.com

Received 16 July 2021; Accepted 20 October 2021

ABSTRACT

With the increasing threat antimony (Sb) pollution poses to the environment, its removal from water is becoming increasingly important. Accordingly, metal-organic frameworks (MOFs) are garnering increasing research attention owing to their excellent performance as adsorbents. Here, the MOF MIL-101(Cr)-NH₂ was prepared directly by solvothermal synthesis. Sb(III) adsorption using MIL-101(Cr)-NH₂ was evaluated systematically at varying adsorbent dosages and pHs. And the adsorption kinetics, isotherms, and thermodynamics were explored by altering the contact time, initial Sb(III) concentration, and temperature, respectively. The results revealed that Sb(III) was adsorbed onto MIL-101(Cr)-NH₂ very quickly, even at low antimony concentrations. The maximum Sb(III) adsorption capacity of MIL-101-NH₂ is 83.61 mg g⁻¹. In the presence of coexisting ion (NO₃⁻), the amount of Sb(III) adsorbed was slightly increased, which may be due to the formation of an inner-sphere complex. The Box–Behnken method was used to design and optimize a response surface with reference to three main influencing factors, that is, dosage, pH, and temperature, so as to obtain a multivariate quadratic model of adsorption behavior and identify the optimal adsorption conditions. Finally, a preliminary economic analysis of the synthetic material was carried out.

Keywords: Antimony; Metal-organic framework; MIL-101(Cr)-NH₂; Adsorption; Coexisting ions; Response surface

1. Introduction

Antimony (Sb) is a naturally occurring metalloid, having the properties of both a metal and a non-metal, and is the fourth element of group VA of the periodic table. It has four oxidation states, and it usually exists as Sb(III) or Sb(V) in environmental media [1]. Most environmental antimony is discharged from pollution sources into the air, water, or soil in the form of Sb₂O₃. Then, it is dissolved and released

into the surrounding media [2]. A number of clinical and laboratory studies on antimony have demonstrated its genotoxic and carcinogenic effects [3,4]. Therefore, the removal of environmental antimony is considered to be a priority, and the World Health Organization (WHO) has stipulated a maximum concentration of Sb in drinking water of 5 µg L⁻¹, while the United States Environmental Protection Agency (USEPA) has designated a maximum Sb contaminant level of 6 µg L⁻¹. Although antimony is harmful, it is

* Corresponding author.

still used in alloys, flame retardants, catalysts, ceramics, and glass [1]. It has been reported that antimony is widely present in fresh and marine waters [5]. In certain water systems, the concentration of antimony exceeds the maximum allowable concentration. Therefore, finding effective methods to remove antimony from water is of crucial importance for the protection of the environment and human health.

Several technologies, including chemical precipitation [6], membrane filtration [7], adsorption [8,9], ion exchange [10], and bioremediation [11], have been evaluated for the removal of antimony from aqueous solutions. Of these, chemical precipitation and adsorption are the most effective, with the remaining methods presenting problems such as high energy consumption, poor selectivity, and poor anti-interference. However, chemical precipitation can cause secondary pollution, and the concentration of heavy metal ions in complex wastewater after such treatment rarely reaches the desired standard, so it is generally only used as a primary pretreatment.

The adsorption method has been used extensively in sewage treatment owing to its simple operation, low energy consumption, and environmental benignity [12]. Adsorption materials that have been studied for the removal of harmful substances in water include graphenes [13], carbon nanofiber [14], and metallic oxides [15,16]. Each of these materials have their own characteristic adsorption properties. Accordingly, with increasing public concern surrounding water safety and the improvement of water quality, the development of efficient and environmentally friendly adsorbent materials has become a key research direction for addressing the antimony pollution problem.

The use of metal-organic frameworks (MOFs) as adsorbents for water treatment is receiving increasing research attention [17,18]. MOFs are a novel family of porous inorganic-organic hybrid materials comprising metal centers and organic linkers [19]. They are simple to synthesize and have large specific surface areas, ordered porous structures, and tunable physiochemical properties, making them highly attractive as adsorbent materials for environmental remediation [20].

As reported previously, the MOF MIL-101 and its derivatives can remove heavy metal ions efficiently from aqueous media [21,22]. MIL-101(Cr) exhibits both thermal and chemical stability owing to the kinetic stability of the Cr compound [23]. And, it has a mesoporous molecular structure with zeolite MTN topology, two different pore sizes, and a large surface area [24]. Furthermore, the pores are sufficiently large to accommodate metal ions and to allow functionalization with organic ligands [22]. Accordingly, amino-functionalized MIL-101(Cr) (MIL-101(Cr)-NH₂) has been extensively studied [25,26]. However, the ability of MIL-101(Cr)-NH₂ to remove Sb(III) from solution has not been previously reported.

In this work, MIL-101(Cr)-NH₂ was prepared by solvothermal synthesis, characterized, and evaluated as an adsorbent for the removal of Sb(III) from aqueous media. The effects of adsorbent dosage, initial pH, and the coexistence of environmentally relevant ions on adsorption performance were assessed, and the adsorption kinetics, isotherms, and thermodynamics were explored by altering the contact time, initial Sb(III) concentration, and temperature. Finally, the

Box-Behnken method was used to design and optimize a response surface with respect to the three main influencing factors, so as to obtain a quadratic model of adsorption behavior and the optimal adsorption conditions. Our study aims to demonstrate that MIL-101(Cr)-NH₂ has broad application prospects as an Sb(III) adsorbent for environmental remediation and provide a foundation for follow-up research.

2. Materials and methods

2.1. Materials

Chromium nitrate nonahydrate (Cr(NO₃)₃·9H₂O, 99%), 2-aminoterephthalic acid (C₈H₇NO₄, 98%), and potassium antimony tartrate (C₄H₄KO₇Sb·0.5H₂O, 98%) were supplied by Shanghai Aladdin Bio-Chem Technology Co., Ltd., (Fengxian District, Shanghai) *N,N*-dimethylformamide (DMF, 99.5%), anhydrous ethanol (CH₃CH₂OH, 99.7%), sodium hydroxide (NaOH, 96%), and hydrochloric acid (HCl, 36%) were supplied by Nanjing Chemical Reagent Co., Ltd., (Liuhe District, Nanjing).

2.2. Preparation of MOFs

MIL-101(Cr)-NH₂ can be prepared by post-synthesis modification of MIL-101(Cr) [27] and directly synthesized by using amino functionalized organic linkers [28,29]. In this work, MIL-101(Cr)-NH₂ was directly fabricated using solvothermal synthesis (Fig. 1).

Briefly, we dissolved 800 mg of Cr(NO₃)₃·9H₂O, 360 mg of 2-aminoterephthalic acid, and 160 mg of NaOH in 75 mL ultrapure water. The solution was ultrasonicated (30 min), then transferred to a Teflon-lined autoclave and heated to 150°C for 12 h. After cooling to room temperature, the mixture was centrifuged (10,000 rpm, 5 min). The product was washed three times with ultrapure water to remove unreacted chromate and sodium hydroxide. After washing, the product was dispersed in DMF and ultrasonicated for 12 h three times. Then, anhydrous ethanol was used to wash the product three times, and it was then heated at 80°C for 6 h. After centrifugation again, the resulting product was dried under vacuum for 12 h at 80°C.

2.3. Characterization

The morphology of MIL-101(Cr)-NH₂ was observed by scanning electron microscopy (SEM; Quanta 400 FEG, FEI Company, Hillsboro, OR, USA). An energy disperse spectroscopy (EDS; Apollo XL, EDAX Inc., Mahwah, NJ, USA) was used to analyze the species and mass distribution of each element on the surface of the sample.

The specific surface area, pore size, and pore volume of the adsorbent were determined using an automated surface area and pore size analyzer (ASAP 2020 HD88, Micromeritics, Norcross, GA, USA). After degassing at 150°C for 24 h, the N₂ adsorption-desorption isotherms of the sample were obtained at -196°C. The specific surface area and pore size were estimated by Brunauer-Emmett-Teller (BET) analysis and density functional theory (DFT), respectively.

X-ray diffraction (XRD; Smartlab 9, Rigaku, Tokyo, Japan) was used to obtain the crystal structure of the sample.



Fig. 1. Synthesis process of MIL-101(Cr)-NH₂.

The power of the Cu-K α X-ray generator was 3 kW, the scanning speed was 0.02°/s, and the 2 θ range was 2°–90°.

Fourier-transform infrared spectroscopy (FTIR; Nicolet IS5, Thermo Scientific, Madison, WI, USA) was performed using potassium bromide pellets with 32 scans (400–4,000 cm⁻¹, 2 cm⁻¹ resolution).

X-ray photoelectron spectrometry (XPS; ESCALAB 250Xi, Thermo Scientific, Madison, WI, USA) was used to analyze the sample surface in terms of element type, valence, and composition.

Thermogravimetric analysis (TGA; 290F3, NETZSCH, Selb, Germany) was performed to determine the thermal stability of the sample under a nitrogen atmosphere (nitrogen flow rate 30 mL min⁻¹, heating rate 10°C min⁻¹, test range room temperature to 800°C).

2.4. Batch experiments

2.4.1. Adsorption experiments

The experiments for assessing the Sb(III) adsorption capacity of MIL-101(Cr)-NH₂ were conducted in a thermostatic oscillation chamber (25°C, 160 rpm). The used adsorbent was removed from solution using a PET syringe filter (0.22 μm), and the Sb(III) concentration of the filtered solution was determined by flame atomic absorption spectroscopy (FAAS) [30]. The Sb(III) adsorption amount and removal rate were calculated from Eqs. (1) and (2):

$$q = \frac{C_0 - C_e}{m} \times V \quad (1)$$

$$R = \frac{C_0 - C_e}{C_0} \times 100\% \quad (2)$$

where q (mg g⁻¹) represents the Sb(III) adsorption amount of the adsorbent at equilibrium; R (%) is the removal rate; C_0 (mg L⁻¹) represents the initial concentration of Sb(III); C_e (mg L⁻¹) represents the concentration of Sb(III) at equilibrium; V (L) represents the solution volume; and m (g) is the mass of adsorbent used.

To investigate the influence of initial pH on antimony adsorption by MIL-101(Cr)-NH₂ and Sb(III) solution

(25 mg L⁻¹) was prepared from potassium antimony tartrate. Then, 0.1 M NaOH and HCl were employed to alter the solution pH to 1, 2, 3, 4, 5, 6, 7, 8, 9, or 10. MIL-101(Cr)-NH₂ (50 mg L⁻¹) was then added to the antimony solution (40 mL), and the mixture was transferred to a centrifuge tube for the adsorption experiment described above for 120 min.

To investigate the effect of adsorbent dosage on Sb(III) adsorption and to obtain the optimal value, MIL-101(Cr)-NH₂ was dosed into 40 mL Sb(III) solution (25 mg L⁻¹) at 50, 100, 150, 200, 250, or 300 mg L⁻¹ (pH 7) and the same experiment was performed.

The coexistence of environmentally relevant ions was also investigated. Sulfamerazine (SM), humic acid (HA), CO₃²⁻, PO₄³⁻, HPO₄²⁻, H₂PO₄⁻ and NO₃⁻ were dosed at initial concentrations of 10 and 100 mg L⁻¹ before adsorption experiments. The MOF (200 mg L⁻¹) and 40 mL Sb(III) solution (25 mg L⁻¹) were added to a centrifuge tube. The solution pH was adjusted to 4 using 0.1 M NaOH and HCl and the mixture was shaken in a thermostatic oscillation chamber at 25°C and 160 rpm for 6 h.

2.4.2. Adsorption kinetics

Kinetic experiments were performed for different contact times. MIL-101(Cr)-NH₂ (200 mg L⁻¹) was added to Sb(III) solution (40 mL, 25 mg L⁻¹). The pH was adjusted to 4 using 0.1 M NaOH and HCl. The mixture was shaken in a thermostatic oscillation chamber at 25°C and 160 rpm for 10, 20, 30, 60, 90, 120, 240, 360, 480, or 720 min. The data were fitted using pseudo-first-order [Eq. (3)], pseudo-second-order [Eq. (4)], intraparticle diffusion [Eq. (5)], and Elovich models [Eq. (6)], and the correlation coefficients (R^2) were used to evaluate model accuracy. The model equations are [31]:

$$\ln(q_{e,\text{exp}} - q_t) = \ln q_{e,\text{cal}} - K_1 t \quad (3)$$

$$\frac{t}{q_t} = \frac{1}{K_2 q_{e,\text{exp}}^2} + \frac{t}{q_{e,\text{cal}}} \quad (4)$$

$$q_t = K_p \cdot t^{0.5} + C \quad (5)$$

$$q_t = b \ln(ab) + b \ln t \quad (6)$$

where q_e (mg g⁻¹) represents the amount of Sb(III) adsorbed at equilibrium concentration; q_t (mg g⁻¹) represents the amount of Sb(III) adsorbed at time t ; t (min) represents contact time; K_1 (min⁻¹) represents the rate constant; K_2 (min⁻¹) is the second-order rate constant; K_p (mg g⁻¹ min^{0.5}) represents the intraparticle diffusion rate constant; C represents the boundary layer thickness; a (mg g⁻¹ min⁻¹) represents the initial adsorption rate constant; and b (mg g⁻¹) represents the desorption rate constant.

2.4.3. Adsorption isotherms

Adsorption isotherm data were obtained by mixing Sb(III) solution (40 mL) of different initial concentrations (5, 10, 25, 50, 100, 150, or 200 mg L⁻¹) and MIL-101(Cr)-NH₂ (200 mg L⁻¹) in a centrifuge tube. The solution pH was adjusted to 4, and the mixture was shaken in a thermostatic oscillation chamber (25°C, 160 rpm, and 6 h). Data were fitted to the Langmuir model [Eq. (7)] and the Freundlich model [Eq. (8)], and the correlation coefficients (R^2) were used to assess model accuracy. The model equations are [32]:

$$\frac{C_e}{q_e} = \frac{1}{q_m K_L} + \frac{C_e}{q_m} \quad (7)$$

$$\ln q_e = \ln K_F + \frac{1}{n} \ln C_e \quad (8)$$

where q_m (mg g⁻¹) represents the maximum monolayer adsorption capacity; K_L represents the Langmuir constant; K_F represents the Freundlich constant; and n represents the heterogeneity factor of adsorption strength.

2.4.4. Adsorption thermodynamics

Critical information about the adsorption process can be obtained from the adsorption thermodynamics [13]. To investigate the effect of temperature, adsorption experiments were performed at 15°C, 25°C, and 35°C. MIL-101(Cr)-NH₂ (200 mg L⁻¹) and 40 mL Sb(III) solution (25 mg L⁻¹) were mixed in a centrifuge tube, and the initial pH was adjusted to 4 with 0.1 M NaOH and HCl. The mixture was shaken in a thermostatic oscillation chamber at 25°C and 160 rpm for 6 h. Gibbs free energy (ΔG), entropy change (ΔS), and enthalpy change (ΔH) were calculated as follows:

$$\Delta G = -RT \ln K \quad (9)$$

$$\Delta G = \Delta H - T \Delta S \quad (10)$$

where R represents the ideal gas constant (8.314 J (mol K)⁻¹); K represents the adsorption equilibrium constant for the best fitting parameters; and T (K) represents the absolute temperature. ΔH and ΔS are the slope and intercept in the fitted plot of Gibbs free energy change (ΔG) vs. temperature (T), respectively.

2.4.5. Response surface optimization

Response surface methodology (RSM) is a statistical method based on rational experimental design whereby multiple quadratic regression equations are used to fit the relationships between influencing factors and response values in order to determine the optimal process parameter values. In this study, the Box–Behnken model was employed for experimental design, and three parameters were established, namely the dosage of adsorbent (X_1), pH (X_2), and initial Sb(III) concentration (X_3). The experimental design factors are presented in Table 1.

The mathematical equation for the adsorption of Sb(III) onto MIL-101(Cr)-NH₂ was established from the interrelation of independent parameters, and it is expressed in the form of a second-order polynomial equation:

$$Y = \beta_0 + \sum_{i=1}^K \beta_i X_i + \sum_{i=1}^K \beta_{ii} X_i^2 + \sum_{i=1}^{K-1} \sum_{j=1}^K \beta_{ij} X_i X_j \quad (11)$$

where Y represents the predicted response for amount of Sb(III) adsorbed; X_i and X_j are independent variables; β_0 represents the offset coefficient; β_i represents the linear coefficient; β_{ii} represents the second-order coefficient; and β_{ij} represents the interaction coefficient.

3. Results and discussion

3.1. Characterization

SEM image showing the surface morphology of MIL-101(Cr)-NH₂ are presented in Fig. 2. MIL-101(Cr)-NH₂ exhibits a roughly regular octahedral crystal morphology, which is consistent with the results of [29]. Fig. 3 shows the chemical composition of MIL-101(Cr)-NH₂ as obtained by EDS.

The N₂ adsorption–desorption isotherm for MIL-101(Cr)-NH₂ is shown in Fig. 4a. The isotherm presents type-I characteristics, indicating that it has a largely microporous structure. In addition, the magnified inset shows that secondary absorption occurs at $P/P_0 = 0.1$ and 0.2, which confirms the existence of two different-sized pore types in the structure (as is consistent with the structure of MIL-101 reported by [24]). The BET specific surface area and total pore volume are approximately 1,022.22 m² g⁻¹ and 0.9085 cm³ g⁻¹, respectively, lower than those of unfunctionalized MIL-101 [22,33,34]. This is presumably due to the introduction of amino groups that prevent guest molecules from accessing some pores [35]. However, while the specific surface area and total pore volume are decreased

Table 1
Experimental design factors for adsorption of Sb(III) by MIL-101(Cr)-NH₂

Factor	Parameters	Levels		
		-1	0	+1
Dosage, mg L ⁻¹	X_1	175	200	225
pH	X_2	3	4	5
Temperature, K	X_3	288.15	298.15	308.15

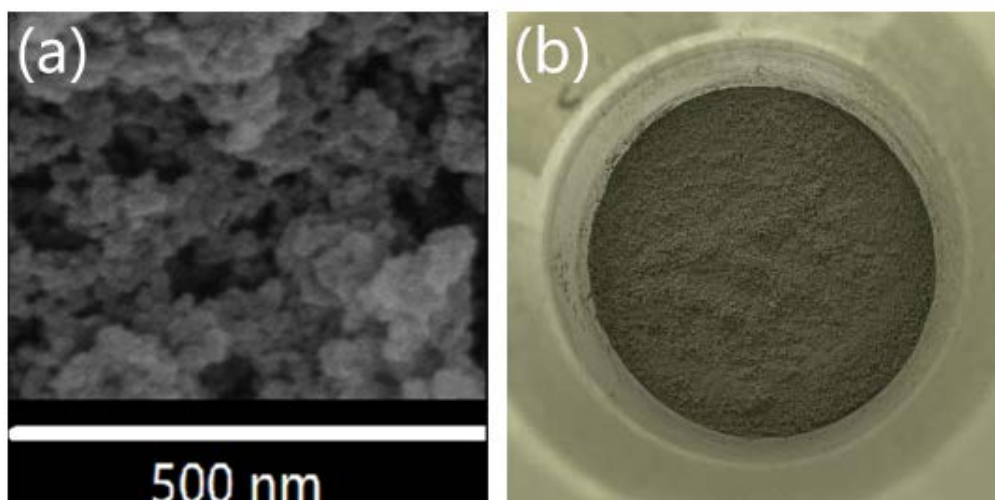


Fig. 2. (a) SEM image and (b) photo of MIL-101(Cr)-NH₂.

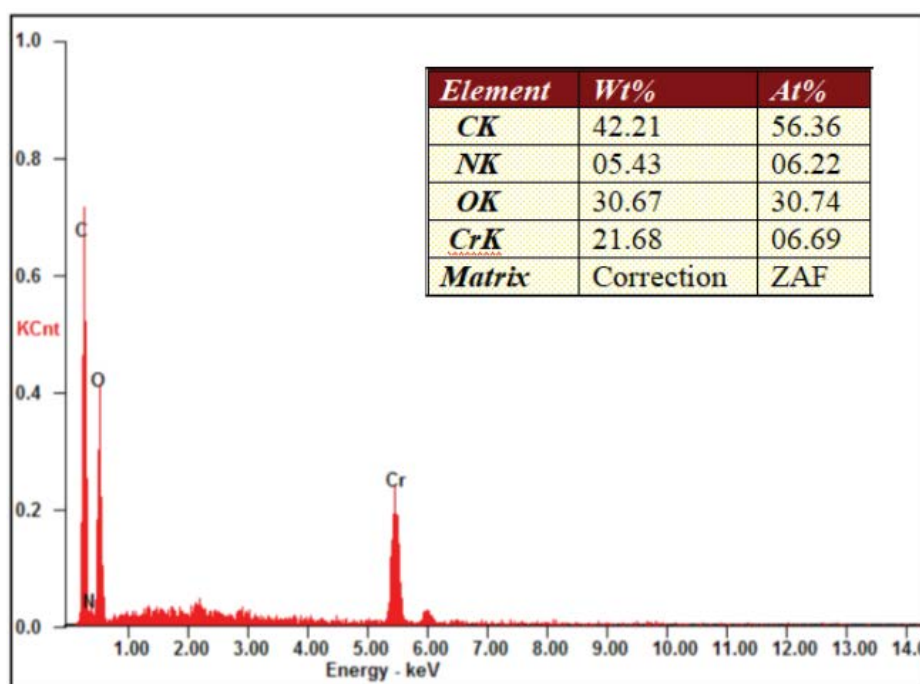


Fig. 3. EDS analysis results and elemental contents of MIL-101(Cr)-NH₂.

upon functionalization, the average pore diameter of MIL-101(Cr)-NH₂ (3.55 nm) is sufficient for access by Sb(III) ions.

The thermal stability of MIL-101(Cr)-NH₂ was also evaluated. The TGA curve (Fig. 4b) shows that the weight loss from MIL-101(Cr)-NH₂ occurs in two steps. The first step that is observed below 200°C is due to loss of guest water molecules. For the second step observed near 300°C, the amino-terephthalic acid ligands decompose and the network structure collapses, resulting in a weight loss of ~70%. These observations are similar to those reported for MIL-101 [33], demonstrating that the thermal stability of MIL-101 is not affected by amino functionalization.

The synthesized adsorbent was also characterized by XRD (Fig. 4c). The sharp diffraction peaks indicate that the sample is highly crystalline, and the pattern has characteristic peaks similar to those previously reported for analogous structures [18,36], indicating the successful construction of MIL-101(Cr)-NH₂.

The FT-IR spectrum of MIL-101-NH₂ is shown in Fig. 4d. A major peak appears at 1,570 cm⁻¹ and a weak double peak appears at 3,385 and 3,419 cm⁻¹, which are attributed to N-H bending, asymmetric N-H vibration, and symmetric stretching, respectively. This confirms the successful introduction of amino functional groups [22].

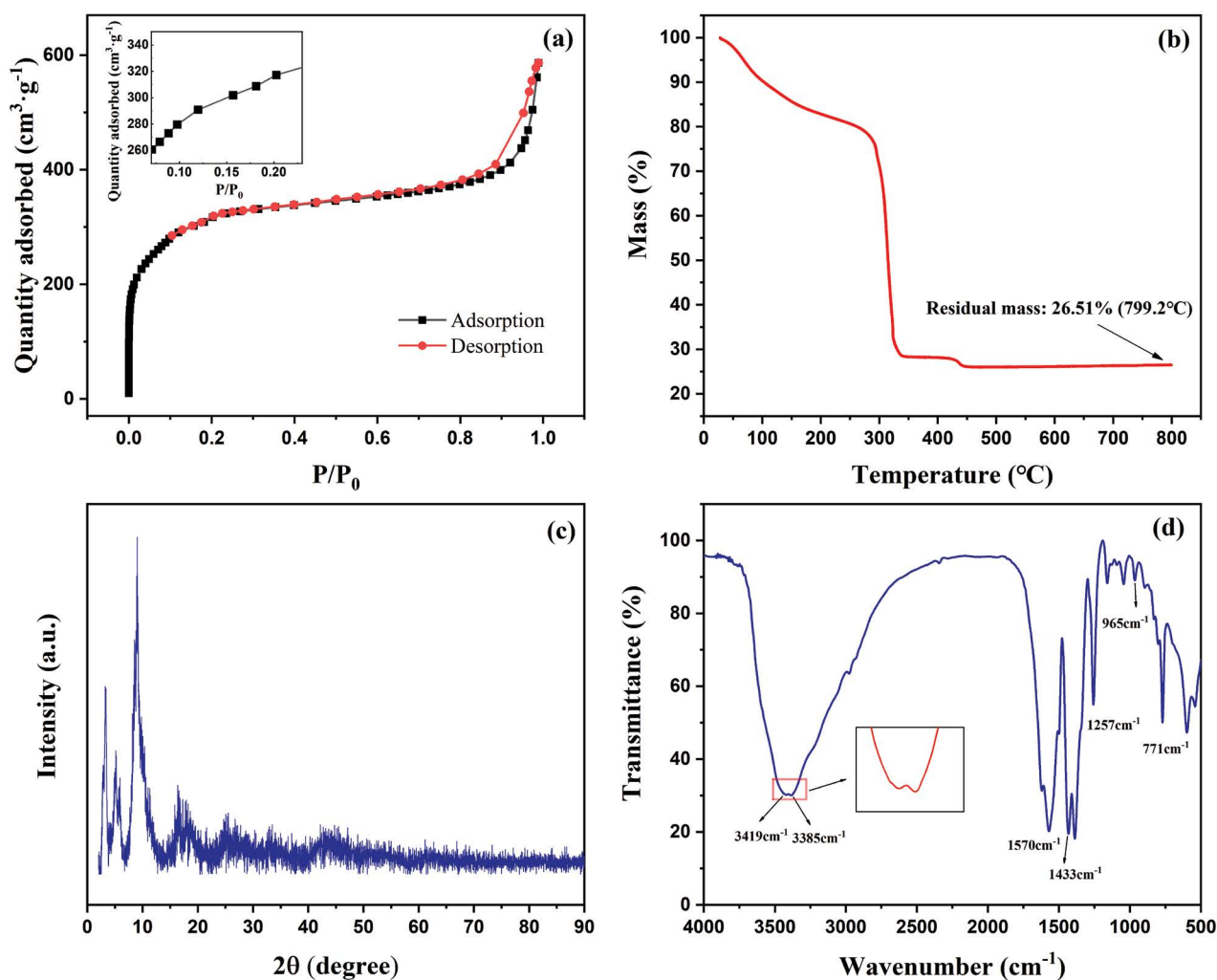


Fig. 4. (a) N_2 adsorption–desorption isotherm, (b) TG curve, (c) XRD pattern, and (d) FT-IR spectrum of MIL-101(Cr)- NH_2 .

There are also peaks at $1,257$ and $1,433\text{ cm}^{-1}$, which could be attributed to aromatic C–N stretching and cleavage vibration. This indicates that there is an intermolecular hydrogen bond between the amino and carboxyl groups in the MOF structure [37]. Additionally, the small peak at 965 cm^{-1} and the sharp peak at 771 cm^{-1} could be due to aromatic C–H bending vibration [29].

The chemical composition and elemental valence states for MIL-101(Cr)- NH_2 were further investigated using XPS. The full survey spectrum of MIL-101(Cr)- NH_2 is given in Fig. 5, demonstrating the presence of C, N, O, and Cr at the atomic mole percentages given in the inset. However, XPS is works to a certain penetration depth. Therefore, the elemental percentages reported may not be the actual values for MIL-101(Cr)- NH_2 [38]. Nevertheless, the results obtained were similar to the elemental percentages detected by EDS.

Fig. 6a shows the C1s spectrum, which can be deconvoluted into peaks at 284.80 , 285.78 , and 288.78 eV that correspond to C–C/C=C, C–N, and C=O bonds, respectively. The C–N bond signals are due to the terephthalic acid ligands in the MIL-101(Cr)- NH_2 structure, which is

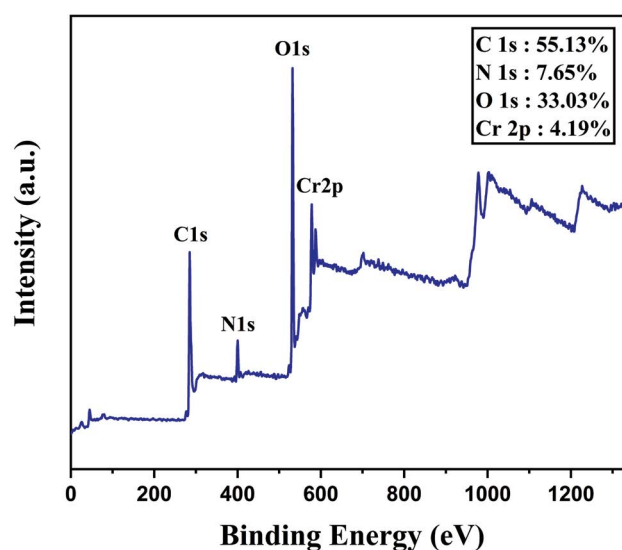


Fig. 5. XPS survey spectrum of MIL-101(Cr)- NH_2 with atomic mole percentages.

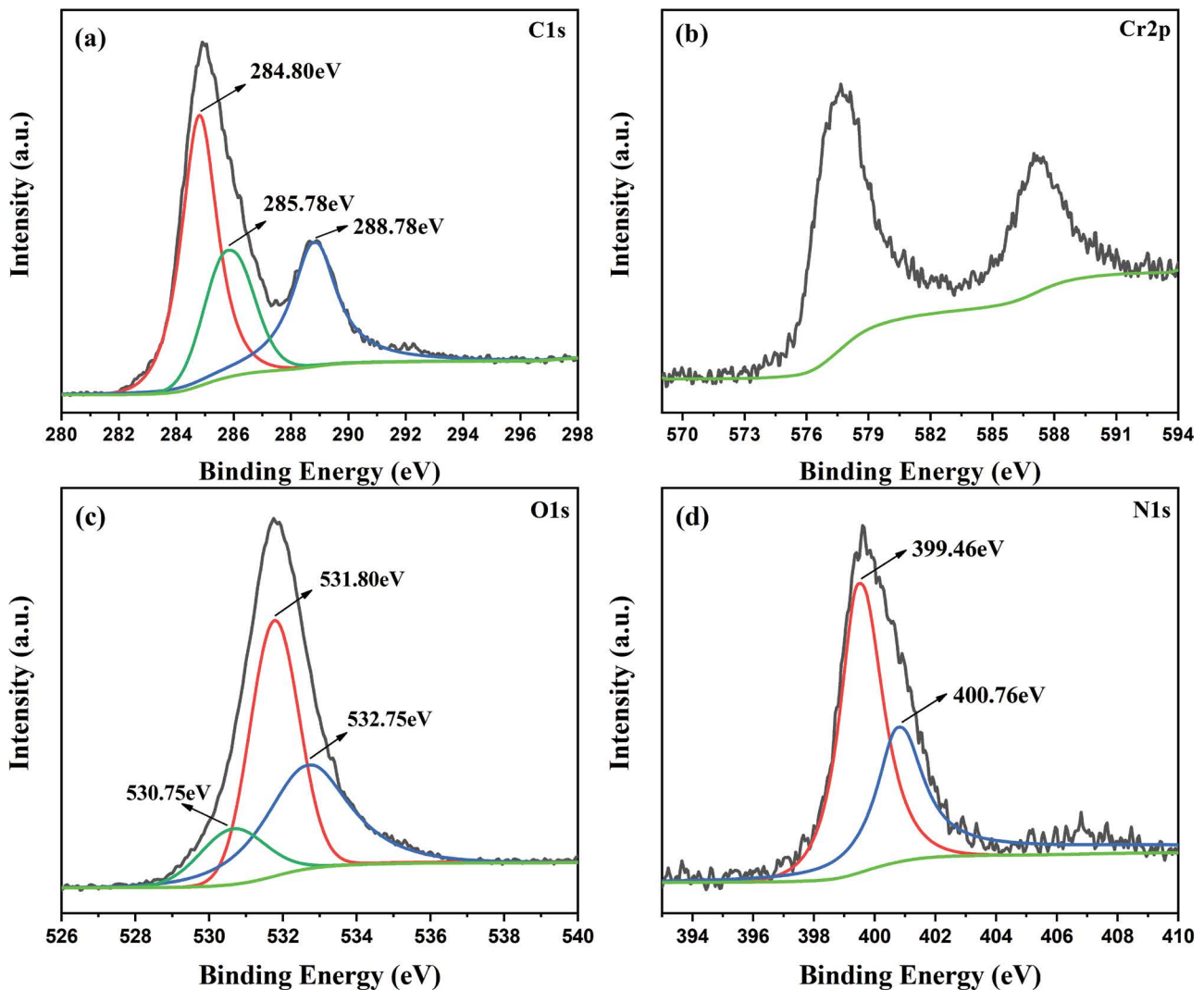


Fig. 6. XPS spectra of MIL-101(Cr)-NH₂: (a) C1s, (b) Cr2p, (c) O1s, and (d) N1s.

consistent with the FT-IR data. The Cr2p spectrum (Fig. 6b) presents peaks for Cr2p_{1/2} and Cr2p_{3/2}. The main peak is observed at 577.59 eV, which evidences the presence of Cr(III) [39]. The O1s spectrum consists of three component peaks at 532.75, 531.8, and 530.75 eV (Fig. 6c), while the N1s spectrum (Fig. 6d) can be deconvoluted into two peaks at 399.46, and 400.76 eV, which are attributed to the N–C and N–H bonds in the amine group, respectively [21]. Thus, these results further confirm the presence of amine groups in MIL-101(Cr)-NH₂.

3.2. Effect of adsorbent dosage

The effect of MIL-101(Cr)-NH₂ dosage on Sb(III) adsorption is shown in Fig. 7a. As the dosage increases from 50 to 200 mg L⁻¹, the amount of Sb(III) adsorbed rapidly increases to a maximum of 27.35 mg g⁻¹, which is mainly because of the increased number of effective adsorption sites [40]. However, with further dosage increase, the amount of Sb(III) adsorbed decreases, which may be caused by a reduction in the concentration of Sb(III) at the MIL-101(Cr)-NH₂

surface, resulting in slower accumulation and diffusion of Sb(III). Accordingly, 200 mg L⁻¹ was adopted as the dose of adsorbent used in this study.

3.3. Effect of pH

Solution pH is a significant factor in the adsorption of metal ions. It affects the chargeability of surface functional groups on the adsorbent and the form of metal ions in the solution [41]. As shown in Fig. 7b, solution pH has a significant effect on the adsorption of Sb(III) by MIL-101(Cr)-NH₂. As the pH increases from 1 to 4, amount of Sb(III) adsorbed increases to its maximal value of 29.5 mg g⁻¹. However, further increase in pH leads to a decrease in adsorption amount. This is because when pH < 4, Sb(III) is partially present as Sb(OH)₂⁺, which experiences electrostatic repulsion with the surface of the positively charged adsorbent [14]. As the pH increases, neutral Sb(OH)₃ becomes dominant, and the influence of electrostatic repulsion decreases. However, as the pH increases from 4 to 10, Sb(III) takes the form of H₂SbO₃ or Sb(OH)₄⁻, which experiences electrostatic

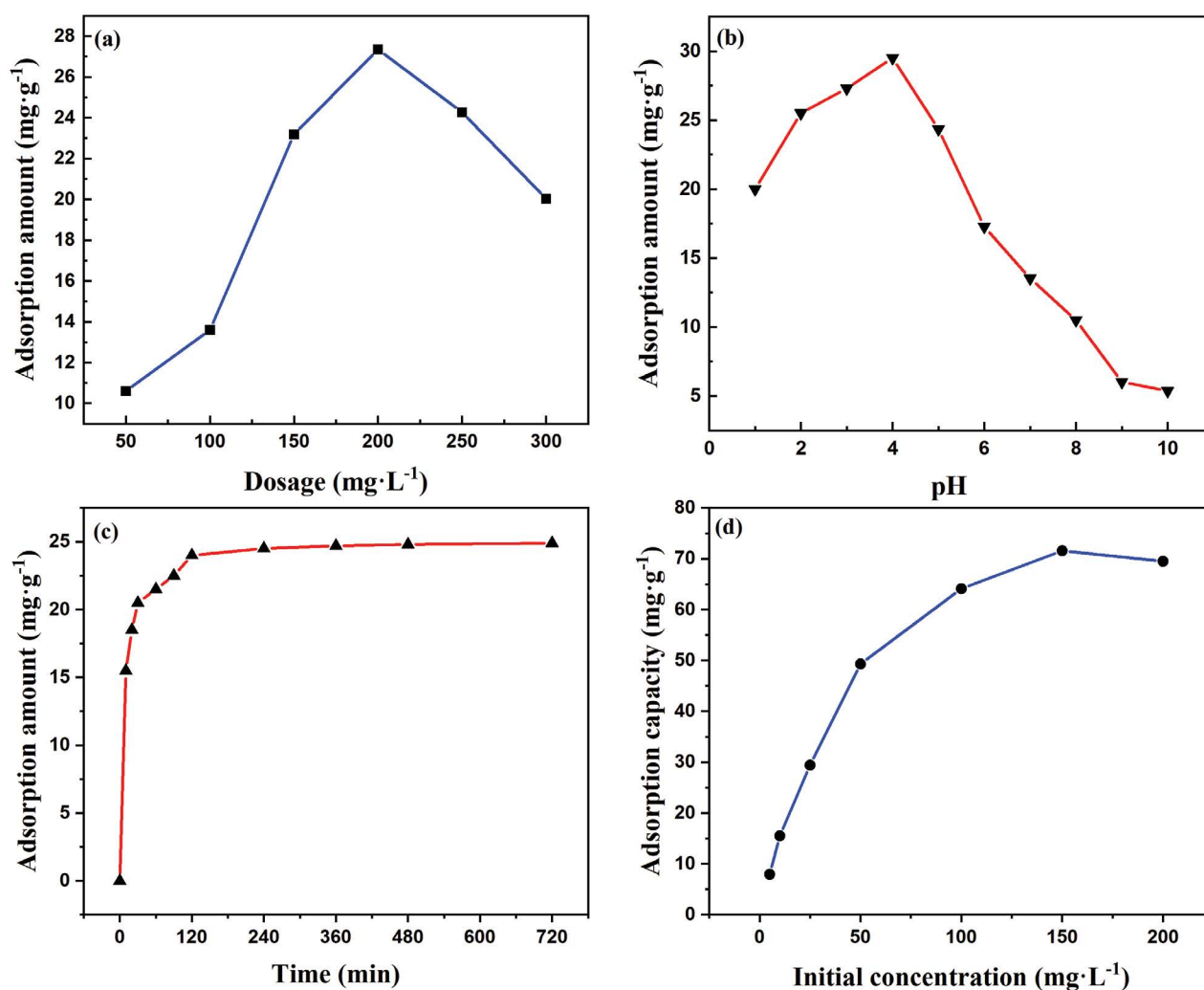


Fig. 7. Effects of (a) adsorbent dosage, (b) initial pH, (c) contact time, and (d) initial Sb(III) concentration on the adsorption amount of MIL-101(Cr)-NH₂.

repulsion with the negatively charged MIL-101(Cr)-NH₂. Moreover, MIL-101(Cr)-NH₂ is formed by the connection of chromium ion metal centers and 2-aminoterephthalic acid organic ligands, and the acidic organic ligands are easily decomposed under higher pH conditions. These factors lead to a decrease in Sb(III) adsorption amount of MIL-101(Cr)-NH₂ under high pH conditions.

3.4. Adsorption kinetics

The effect of contact time on Sb(III) adsorption by MIL-101(Cr)-NH₂ is shown in Fig. 7c. In the first 30 min, the Sb(III) adsorption amount increases rapidly to 20.5 mg g⁻¹ due to the initial abundance of free adsorption sites on MIL-101(Cr)-NH₂. Thereafter, the adsorption curve plateaus and approaches equilibrium at around 120 min due to saturation of the adsorption sites. At equilibrium, the Sb(III) adsorption amount of MIL-101(Cr)-NH₂ is 24.9 mg g⁻¹.

Pseudo-first-order, pseudo-second-order, Elovich, and intraparticle diffusion models were used to analyze the kinetics of Sb(III) adsorption on MIL-101(Cr)-NH₂.

Correlation coefficients (R^2) were used to evaluate the goodness of fit between the experimental data and the model. Fig. 8 shows the plots for the different models, and Table 2 lists their various kinetic parameters. The R^2 values for the pseudo-first-order, pseudo-second-order, and Elovich models are 0.879, 0.999, and 0.906, respectively. Clearly, the pseudo-first-order and Elovich models are not accurate kinetic descriptions of the adsorption of Sb(III) on MIL-101(Cr)-NH₂, whereas the pseudo-second-order model is applicable to this adsorption process. The results obtained by linear fitting also present the same conclusion, that is, the equilibrium adsorption amount ($q_{e,cal}$) calculated using pseudo-second-order kinetics more closely resembles the experimental result ($q_{e,exp}$). The pseudo-second-order model is based on the assumption that the adsorption rate is controlled by chemical adsorption [42]. Thus, our results indicate that Sb(III) adsorption on MIL-101(Cr)-NH₂ is a chemical adsorption process.

Sb(III) diffusion from the solution into the pores of MIL-101(Cr)-NH₂ involves three main stages: Ions diffuse from the solution into the vicinity of the adsorbent, diffuse from

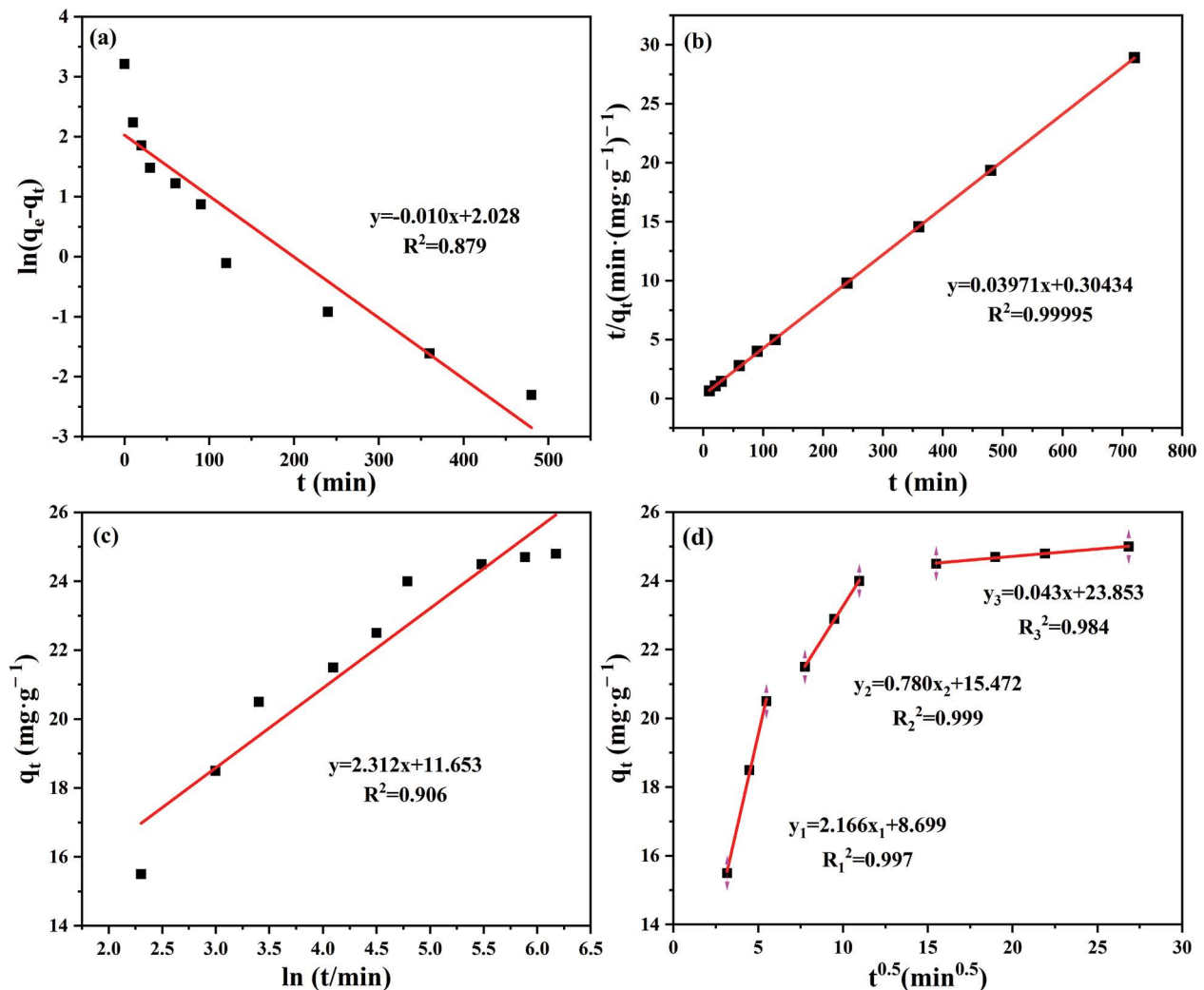


Fig. 8. Adsorption kinetics of Sb(III) on MIL-101(Cr)-NH₂. (a) Pseudo-first-order, (b) pseudo-second-order, (c) Elovich, and (d) intraparticle diffusion models.

the layer around the adsorbent to the surface of adsorbent, and diffuse from the surface to the internal sites [31]. In this intraparticle diffusion model, there are also three stages in the adsorption process, namely mass transfer, adsorption, and diffusion. The correlation coefficients for these three stages are 0.997, 0.999, and 0.984, respectively, showing a good fit to the intraparticle diffusion model. In addition, the slopes of the three stages are 2.166, 0.780, and 0.043, respectively, indicating that the intraparticle diffusion is slower than external diffusion. Moreover, none of the fitted lines cross the origin, indicating that there are other rate-controlling steps besides intraparticle diffusion.

3.5. Adsorption isotherms

The effect of initial Sb(III) concentration on its adsorption by MIL-101(Cr)-NH₂ is shown in Fig. 7d. As the initial concentration was increased from 5 to 150 mg L⁻¹, the adsorption amount increased, which is attributed to the increasing ion concentration producing the driving force

that overcomes mass transfer resistance. At low initial concentrations of Sb(III), MIL-101-NH₂ has a significant adsorption effect, indicating that it has a strong affinity for trace antimony ions. For practical application, this is of great significance, since the removal of trace-level Sb(III) in actual water largely depends on adsorption effectiveness rather than adsorption capacity. MIL-101(Cr)-NH₂ also exhibits excellent Sb(III) adsorption at high concentrations. Therefore, MIL-101(Cr)-NH₂ shows great promise for practical application to environmental remediation.

In order to learn more about the adsorption behavior, the adsorption data were fitted to Langmuir and Freundlich isotherm models. The fitting curves for the two models are shown in Fig. 9. According to the adsorption data, the correlation coefficients (R^2) for the Langmuir and Freundlich models are 0.992 and 0.959, respectively. Therefore, the Langmuir model is a more accurate representation of the adsorption process, indicating that antimony adsorption occurs at the binding sites on the surface of MIL-101(Cr)-NH₂, which is regarded as monolayer adsorption [43].

The Freundlich constant (n^{-1}) indicates the correlation between the adsorption intensity and heterogeneity of a material and can be used as an index of favorable adsorption [44]. As shown in Table 3, the calculated Freundlich constant is 0.54 (less than 1), indicating that this material has a favorable adsorption effect on Sb(III). Furthermore, according to Eq. (7), the theoretical maximum Sb(III) adsorption capacity of MIL-101(Cr)-NH₂ is 83.61 mg g⁻¹, higher than many adsorbents reported previously (Table 4).

Table 2
Kinetic parameters for the adsorption of Sb(III) by MIL-101(Cr)-NH₂

Model	Parameter	MIL-101(Cr)-NH ₂
Pseudo-first-order	$q_{e,exp}$ (mg g ⁻¹)	24.90
	$q_{e,cal}$ (mg g ⁻¹)	7.60
	K_1 (min ⁻¹)	0.010
	R^2	0.879
Pseudo-first-order	$q_{e,exp}$ (mg g ⁻¹)	24.90
	$q_{e,cal}$ (mg g ⁻¹)	25.18
	K_2 (min ⁻¹)	0.005
	R^2	0.999
Elovich	a	66.766
	b	2.312
	R^2	0.906
Intraparticle diffusion	K_{p1} (mg g ⁻¹ h ^{-0.5})	2.166
	C_1	8.697
	R_1^2	0.997
	K_{p2} (mg g ⁻¹ h ^{-0.5})	0.780
	C_2	15.472
	R_2^2	0.999
	K_{p3} (mg g ⁻¹ h ^{-0.5})	0.043
C_3	23.853	
	R_3^2	0.984

3.6. Adsorption thermodynamics

Thermodynamic analysis is a useful tool for exploring the spontaneity and mechanism of a reaction process. In this study, the ΔG , ΔH , and ΔS values for the adsorption process at 288.15, 298.15, and 308.15 K were derived using Eqs. (9) and (10) (Table 5). The ΔG values are -0.82, -0.62, and -0.38 kJ mol⁻¹, respectively. The negative ΔG values reveal that the adsorption process is spontaneous. Furthermore, with decreasing temperature, the value of ΔG decreases, which indicates that the spontaneity of the adsorption increases with decreasing temperature.

The values of ΔH and ΔS are -7.29 kJ mol⁻¹ and 22 J mol⁻¹ K⁻¹, respectively. The negative ΔH value indicates that the process is exothermic, while the positive value of ΔS demonstrates that the adsorbed Sb(III) is disordered and the randomness at the solid-liquid interface is enhanced during adsorption [51].

3.7. Effects of coexisting ions

The composition of natural water is typically complicated. Thus, various components will be copresent with environmental Sb(III), which may affect its interaction with an adsorbent. Accordingly, the effects of SM, HA, PO₄³⁻,

Table 3
Parameters related to isotherm models of Sb(III) adsorption by MIL-101(Cr)-NH₂

Model	Parameter	MIL-101(Cr)-NH ₂
Langmuir	q_m (mg g ⁻¹)	83.61
	R^2	0.992
Freundlich	K_L	0.040
	n^{-1}	0.540
	R^2	0.950
	K_f	5.820

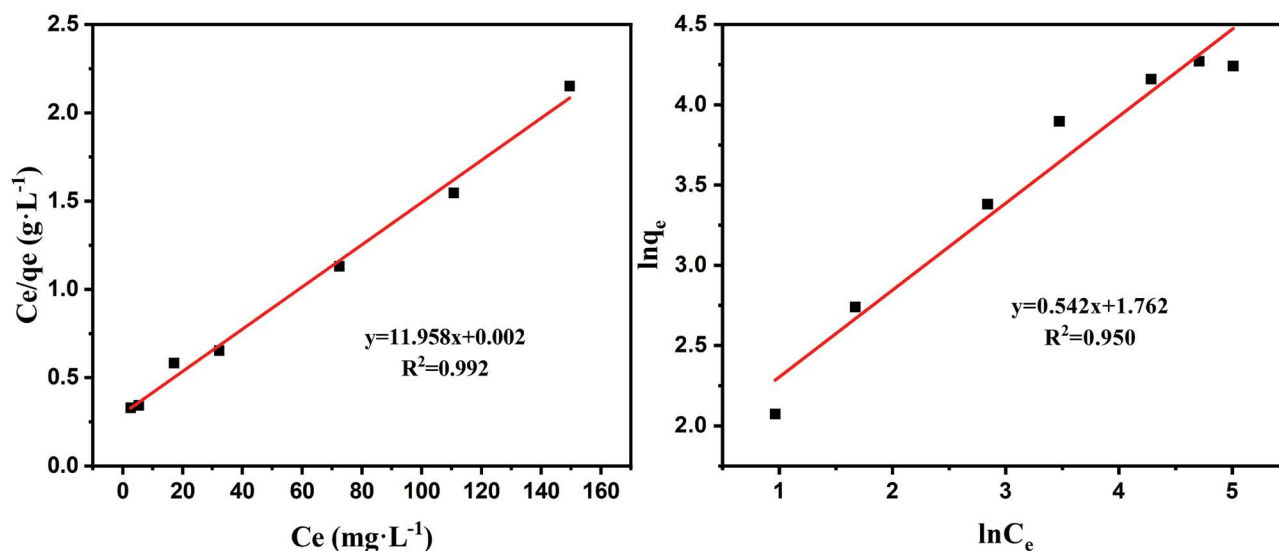


Fig. 9. (a) Langmuir model and (b) Freundlich model of Sb(III) adsorption by MIL-101(Cr)-NH₂.

Table 4
Performance data for different adsorbents reported in the literature

Adsorbents	Initial concentration range (mg L ⁻¹)	pH	Adsorption capacity (mg g ⁻¹)	Reference
UIO-66-NH ₂	10–600	1.5–12	64.89	[45]
Graphene	1–10	3–10	7.46	[46]
ZCN	10–500	7.0	70.83	[14]
Cu-Fe ₃ O ₄	5–100	7.0	43.55	[47]
PHMSs	0.004–0.012	6.0	117.64	[48]
Fe-ATP bead	1–100	1–11	39.24	[49]
Nano-modified Chitosan	5–80	11	52.91	[50]
MIL-101(Cr)-NH ₂	5–200	4.0	83.61	This work

Table 5
Thermodynamic parameters for Sb(III) adsorption on MIL-101(Cr)-NH₂

Adsorbent	T (K)	ΔG (kJ mol ⁻¹)	ΔH (kJ mol ⁻¹)	ΔS (J (mol K) ⁻¹)
MIL-101 (Cr)-NH ₂	288.15	-0.82	-7.29	22
	298.15	-0.62		
	308.15	-0.38		

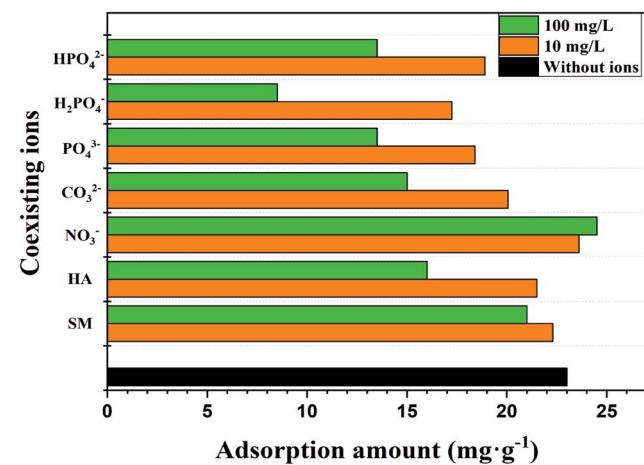


Fig. 10. Effects of coexisting ions on Sb(III) adsorption by MIL-101(Cr)-NH₂.

HPO₄²⁻, H₂PO₄⁻, CO₃²⁻, and NO₃⁻ on adsorption were investigated. The experimental concentrations of these ions were set at 10 and 100 mg L⁻¹. As shown in Fig. 10, when copresent with 10 mg L⁻¹ SM and HA, the adsorption of Sb(III) decreases by 3% and 15%, respectively, due to competition between the ions. In the presence of PO₄³⁻ and CO₃²⁻, adsorption is obviously reduced. The structures of HPO₄²⁻ and H₂PO₄⁻ ions are similar to that of PO₄³⁻ and they also have a clear inhibitory effect on Sb(III) adsorption, which is consistent with previously reported results [52]. This is possibly due to the fact that phosphorus and antimony belong to the same group of the periodic table and thus have similar atomic structures, leading to competition between phosphorus and antimony for the same adsorption sites. However,

Table 6
Results of Box–Behnken design for the adsorption of Sb(III) by MIL-101(Cr)-NH₂

Run	Level (input variable)			Response variable	
	X ₁	X ₂	X ₃	q _{exp} (mg g ⁻¹)	q _{pred} (mg g ⁻¹)
1	-1	-1	0	23.28	24.72
2	1	-1	0	24.03	27.40
3	-1	1	0	24.43	27.82
4	1	1	0	27.38	28.30
5	-1	0	-1	28.11	30.54
6	1	0	-1	28.86	31.56
7	-1	0	1	24.85	26.70
8	1	0	1	26.72	28.84
9	0	-1	-1	27.85	27.44
10	0	1	-1	28.25	28.08
11	0	-1	1	22.63	22.80
12	0	1	1	25.75	26.16
13	0	0	0	28.10	28.07
14	0	0	0	27.94	28.07
15	0	0	0	28.22	28.07
16	0	0	0	28.11	28.07
17	0	0	0	27.98	28.07

in the presence of 10 and 100 mg L⁻¹ NO₃⁻, the adsorption amount increases by 2.6% and 6.5%, respectively. According to conclusions drawn previously [16,53], as the concentration of coexisting ions increases, and if ionic strength has a favorable or minimal effect on Sb(III) adsorption amount, an inner-sphere complex may be formed.

In general, when the dosage of the coexisting ions is 10 mg L⁻¹, little effect on Sb(III) adsorption is observed. Consequently, the adsorption mechanism may be based on the process of ion exchange with an inner-sphere complex.

3.8. Response surface optimization

The results of Box–Behnken design for the adsorption of Sb(III) are shown in Table 6. The quadratic polynomial relationship between the predicted response of adsorption amount and the independent variable is exhibited below:

$$\begin{aligned}
 Y = & 28.07 + 0.79X_1 + X_2 - 1.64X_3 \\
 & - 0.55X_1X_2 + 0.28X_1X_3 + 0.68X_2X_3 \\
 & + 1.44X_1^2 - 2.15X_2^2 + 0.202X_3^2
 \end{aligned}
 \tag{12}$$

Table 7 lists the of ANOVA values for the adsorption conditions. The results show that both the *F*-value and *P*-value are acceptable, which indicates that the proposed quadratic model has statistical significance.

Fig. 11 shows the normal plot of residuals within the response process. It can be observed from this linear distribution that the variance is not very variable, which indicates that the prediction model has a high degree of fitting. Fig. 12 shows the adsorption anomaly curve for the adsorption of Sb(III) on MIL-101(Cr)-NH₂. The residual values of all the experimental runs are distributed randomly

Table 7
ANOVA data for the adsorption conditions

Source	Sum of squares	DOF	Mean square	F-value	P-value
Model	64.04	9	7.12	50.38	<0.0001
X ₁	4.99	1	4.99	35.35	0.0006
X ₂	8.04	1	8.04	56.93	0.0001
X ₃	21.52	1	21.52	152.35	<0.0001
X ₁ X ₂	1.21	1	1.21	8.57	0.0221
X ₁ X ₃	0.3136	1	0.3136	2.22	0.1798
X ₂ X ₃	1.85	1	1.85	13.1	0.0085
(X ₁) ²	5.45	1	5.45	38.57	0.0004
(X ₂) ²	19.51	1	19.51	138.13	<0.0001
(X ₃) ²	0.1727	1	0.1727	1.22	0.3054

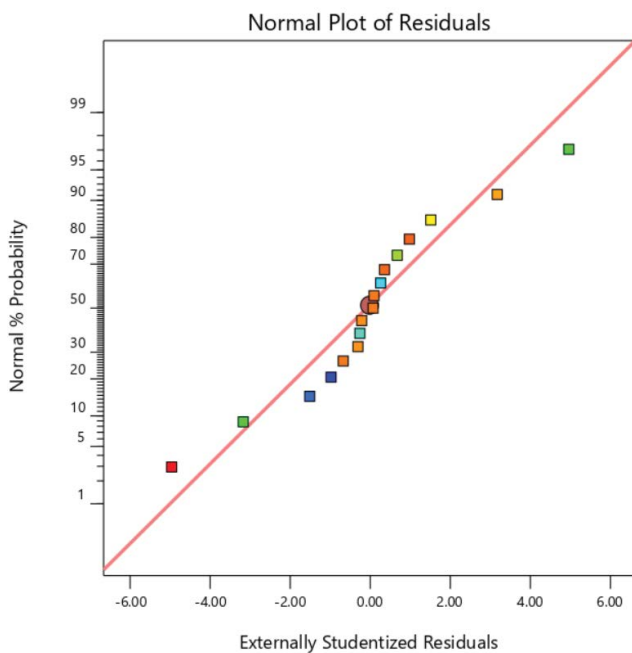


Fig. 11. Normal plot of the residuals in the response process.

in the range -4 – 4 and no outliers are observed, which supports the accuracy of the model prediction.

Fig. 13 show the 3D surfaces and contour lines of the effects of different parameters on Sb(III) adsorption by MIL-101(Cr)-NH₂. All three contour lines are nearly elliptical in shape, which indicates that there are certain interaction relationships between dosage and pH value, temperature and dosage, and pH value and temperature. According to the model, the optimal conditions for Sb(III) adsorption are: dosage = 235.18 mg L⁻¹, pH = 3.63, and temperature = 294.39 K, and the predicted maximum Sb(III) adsorption amount is 29.97 mg g⁻¹.

To verify the optimized conditions, the data from the verification experiment was compared with the model prediction data, revealing that the deviation between the predicted value and the measured value (28.62 mg g⁻¹) is ~4.7% under the optimal conditions. This indicates that the response surface optimization model for Sb(III) adsorption by MIL-101(Cr)-NH₂ is highly compatible.

3.9. Economic analysis

Despite their great potential for the adsorption of heavy metal ions, the synthesis of MOFs is currently only carried out at the laboratory scale. Accordingly, we conducted a preliminary economic evaluation of antimony adsorption by MIL-101(Cr)-NH₂. To obtain a more intuitive result, only the costs of production were considered. Unlike the small-batch purchases typically used for laboratory-scale production, chemicals are usually purchased in large quantities for actual industrial production, and buying chemicals in bulk can reduce production costs. According to the price of chemical agents on the alibaba.com website in March 2021, the cost of batch synthesis of 1 kg MIL-101(Cr)-NH₂ would cost ~327 USD. However, organic solvents can be recovered through drying and filtration, and the recycling rate

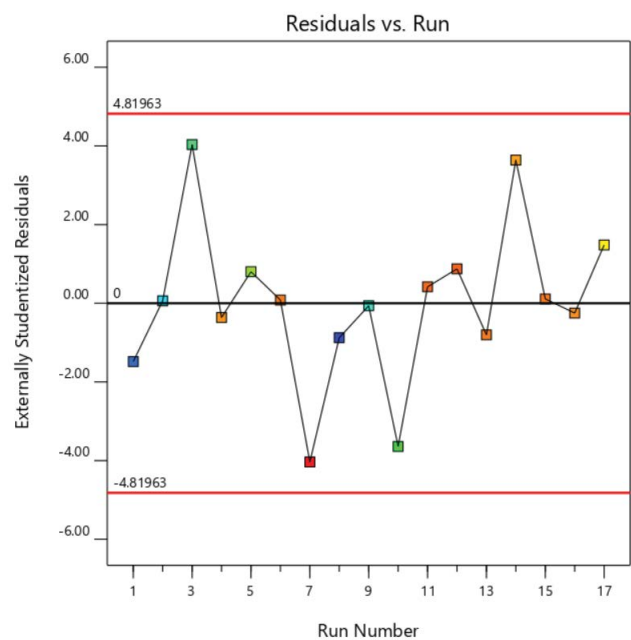


Fig. 12. Adsorption anomaly curve during response.

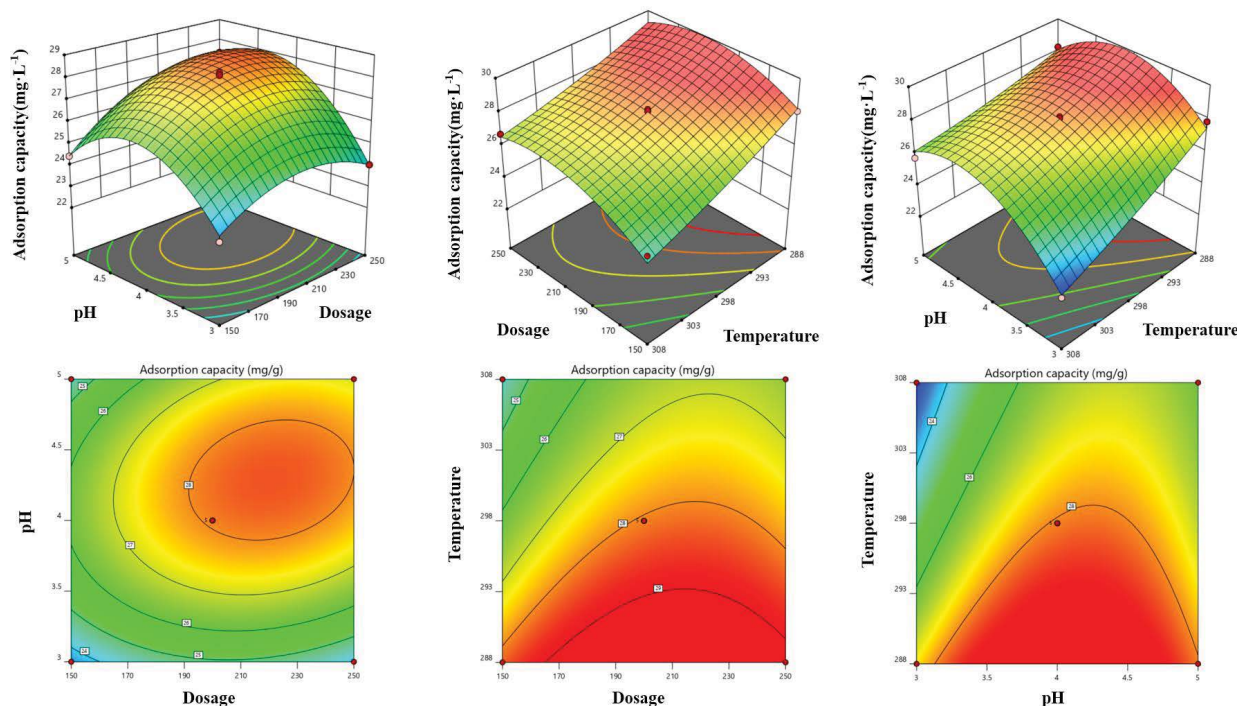


Fig. 13. 3D surfaces and contour lines of the effects of different parameters on Sb(III) adsorption by MIL-101(Cr)-NH₂.

is generally 90% [54]. Ignoring the energy consumption of the recycling process, the revised cost for the production of 1 kg of MIL-101(Cr)-NH₂ is 69.16 USD. Thus, according to the optimal MIL-101(Cr)-NH₂ dosage of 235.18 mg L⁻¹, the cost of treating wastewater with an antimony concentration of 25 mg L⁻¹ is 16.25 USD/t.

Furthermore, MIL-101(Cr)-NH₂ as a solid adsorbent has advantages over liquid materials in terms of storage and transportation costs. Most of its production cost lies in the organic solvents used to wash the synthetic material. However, it has been proposed that certain MOFs can be synthesized in an aqueous solution-based systems [55]. For situations where it is impossible to replace organic solvents with aqueous solutions, it is necessary to replace the organic solvent with water in the washing step or to maximize the recycling efficiency of the organic solvent to reduce the estimated cost [56]. At present, MOFs are mainly limited by high production costs, so they have few industrial applications. However, if the synthesis costs can be effectively reduced in future research, MOFs will become more widely applied in the field of adsorption.

4. Conclusions

In this study, MIL-101(Cr)-NH₂ was successfully prepared by solvothermal synthesis and used to adsorb Sb(III) effectively. Single-factor batch adsorption experiments were performed under different conditions, revealing that the optimal adsorbent dosage and solution pH are 200 mg L⁻¹ and 4, respectively.

Under different pH conditions, Sb exists as different ionic compounds in solution, which is the main factor affecting the adsorption process. The amount of Sb(III) adsorbed by

MIL-101(Cr)-NH₂ can reach 80% of the maximum adsorption amount within 30 min. Furthermore, MIL-101-NH₂ also had a significant adsorption effect at low initial concentrations of Sb(III), indicating that it has a strong affinity for trace antimony ions.

The kinetics and isotherm data were best fitted with pseudo-second-order and Langmuir models, respectively. The maximum Sb(III) adsorption capacity of MIL-101-NH₂ is 83.61 mg g⁻¹. Furthermore, thermodynamic analysis indicated that the process is spontaneous and exothermic.

When Sb(III) is copresent with environmentally relevant ions such as PO₄³⁻ and CO₃²⁻, competitive adsorption results in a decrease in adsorption amount, while adsorption is slightly improved in the presence of NO₃⁻. This indicates that the adsorption mechanism may be based on the process of ion exchange with an inner-sphere complex.

In the multi-factor response surface optimization, we obtained a multiple quadratic regression equation relating the factors and the response value, as well as the optimal adsorption conditions (235.18 mg L⁻¹, pH 3.63, 294.39 K). The deviation between the measured value and the predicted value is ~4.7% under the optimal conditions, which shows that the response surface optimization model is highly compatible and could be used to optimize the experimental conditions.

Although the production of MIL-101(Cr)-NH₂ is currently limited by cost, it remains a promising adsorbent for antimony removal from water due to its excellent performance.

Acknowledgments

The authors express their sincere gratitude to the National Key Research and Development Program of China (No. 2018YFC0408000, 2018YFC0408004) for financial support.

References

- [1] M. Filella, N. Belzile, Y.W. Chen, Antimony in the environment: a review focused on natural waters I. Occurrence, *Earth Sci. Rev.*, 57 (2002) 125–176.
- [2] M. He, X. Wang, F. Wu, Z. Fu, Antimony pollution in China, *Sci. Total Environ.*, 421 (2012) 41–50.
- [3] S. Sundar, J. Chakravarty, Antimony toxicity, *Int. J. Environ. Res. Public Health*, 7 (2010) 4267–4277.
- [4] Z. Zhang, N. Zhang, H. Li, Y. Lu, Z. Yang, Potential health risk assessment for inhabitants posed by heavy metals in rice in Zijiang River basin, Hunan Province, China, *Environ. Sci. Pollut. Res.*, 27 (2020) 24013–24024.
- [5] M.C. He, N.N. Wang, X.J. Long, C.J. Zhang, C.L. Ma, Q.Y. Zhong, A.H. Wang, Y. Wang, A. Pervaiz, J. Shan, Antimony speciation in the environment: recent advances in understanding the biogeochemical processes and ecological effects, *J. Environ. Sci.*, 75 (2019) 14–39.
- [6] Y.L. Liu, Z.M. Lou, K.L. Yang, Z.N. Wang, C.C. Zhou, Y.Z. Li, Z. Cao, X.H. Xu, Coagulation removal of Sb(V) from textile wastewater matrix with enhanced strategy: comparison study and mechanism analysis, *Chemosphere*, 237 (2019) 124494, doi: 10.1016/j.chemosphere.2019.124494.
- [7] L. Meng, M. Wu, H. Chen, Y. Xi, M. Huang, X. Luo, Rejection of antimony in dyeing and printing wastewater by forward osmosis, *Sci. Total Environ.*, 745 (2020) 141015, doi: 10.1016/j.scitotenv.2020.141015.
- [8] W. Zhao, B. Ren, A. Hursthouse, Z. Wang, Facile synthesis of nanosheet-assembled gamma-Fe₂O₃ magnetic microspheres and enhanced Sb(III) removal, *Environ. Sci. Pollut. Res.*, 28 (2021) 19822–19837.
- [9] X. He, X. Min, T. Peng, Y. Ke, F. Zhao, M. Sillanpaa, Y. Wang, Enhanced adsorption of antimonate by ball-milled microscale zero valent iron/pyrite composite: adsorption properties and mechanism insight, *Environ. Sci. Pollut. Res.*, 27 (2020) 16484–16495.
- [10] A.S.C. Chen, L. Wang, T.J. Sorg, D.A. Lytle, Removing arsenic and co-occurring contaminants from drinking water by full-scale ion exchange and point-of-use/point-of-entry reverse osmosis systems, *Water Res.*, 172 (2020) 115455, doi: 10.1016/j.watres.2019.115455.
- [11] N. Van Khanh, Y. Park, T. Lee, Microbial antimonate reduction with a solid-state electrode as the sole electron donor: a novel approach for antimony bioremediation, *J. Hazard. Mater.*, 377 (2019) 179–185.
- [12] J. Wen, Y. Fang, G. Zeng, Progress and prospect of adsorptive removal of heavy metal ions from aqueous solution using metal-organic frameworks: a review of studies from the last decade, *Chemosphere*, 201 (2018) 627–643.
- [13] T.A. Saleh, A. Sari, M. Tuzen, Effective adsorption of antimony(III) from aqueous solutions by polyamide-graphene composite as a novel adsorbent, *Chem. Eng. J.*, 307 (2017) 230–238.
- [14] J.M. Luo, X.B. Luo, J. Crittenden, J.H. Qu, Y.H. Bai, Y. Peng, J.H. Li, Removal of antimonite (Sb(III)) and antimonate (Sb(V)) from aqueous solution using carbon nanofibers that are decorated with zirconium oxide (ZrO₂), *Environ. Sci. Technol.*, 49 (2015) 11115–11124.
- [15] W. Xu, H. Wang, R. Liu, X. Zhao, J. Qu, The mechanism of antimony(III) removal and its reactions on the surfaces of Fe-Mn binary oxide, *J. Colloid Interface Sci.*, 363 (2011) 320–326.
- [16] X. Guo, Z. Wu, M. He, X. Meng, X. Jin, N. Qiu, J. Zhang, Adsorption of antimony onto iron oxyhydroxides: adsorption behavior and surface structure, *J. Hazard. Mater.*, 276 (2014) 339–345.
- [17] C. Wang, J. Luan, C. Wu, Metal-organic frameworks for aquatic arsenic removal, *Water Res.*, 158 (2019) 370–382.
- [18] W. Zhang, N. Li, T. Xiao, W.T. Tang, G.L. Xiu, Removal of antimonite and antimonate from water using Fe-based metal-organic frameworks: the relationship between framework structure and adsorption performance, *J. Environ. Sci.*, 86 (2019) 213–224.
- [19] H. Furukawa, K.E. Cordova, M. O’Keeffe, O.M. Yaghi, The chemistry and applications of metal-organic frameworks, *Science*, 341 (2013) 1230444. doi: 10.1126/science.1230444.
- [20] S. Sadeghian, H. Pourfakhar, M. Baghdadi, B. Aminzadeh, Application of sand particles modified with NH₂-MIL-101(Fe) as an efficient visible-light photocatalyst for Cr(VI) reduction, *Chemosphere*, 268 (2021) 129365, doi: 10.1016/j.chemosphere.2020.129365.
- [21] S.-W. Lv, J.-M. Liu, C.-Y. Li, N. Zhao, Z.-H. Wang, S. Wang, A novel and universal metal-organic frameworks sensing platform for selective detection and efficient removal of heavy metal ions, *Chem. Eng. J.*, 375 (2019) 122111, doi: 10.1016/j.cej.2019.122111.
- [22] Y.-R. Lee, K. Yu, S. Ravi, W.-S. Ahn, Selective adsorption of rare earth elements over functionalized Cr-MIL-101, *ACS Appl. Mater. Interfaces*, 10 (2018) 23918–23927.
- [23] G. Ferey, C. Mellot-Draznieks, C. Serre, F. Millange, J. Dutour, S. Surble, I. Margiolaki, A chromium terephthalate-based solid with unusually large pore volumes and surface area, *Science*, 309 (2005) 2040–2042.
- [24] D.Y. Hong, Y.K. Hwang, C. Serre, G. Ferey, J.S. Chang, Porous chromium terephthalate MIL-101 with coordinatively unsaturated sites: surface functionalization, encapsulation, sorption and catalysis, *Adv. Funct. Mater.*, 19 (2009) 1537–1552.
- [25] L. Fu, S. Wang, G. Lin, L. Zhang, Q. Liu, J. Fang, C. Wei, G. Liu, Post-functionalization of UiO-66-NH₂ by 2,5-Dimercapto-1,3,4-thiadiazole for the high efficient removal of Hg(II) in water, *J. Hazard. Mater.*, 368 (2019) 42–51.
- [26] L. Ding, P. Shao, Y. Luo, X. Yin, S. Yu, L. Fang, L. Yang, J. Yang, X. Luo, Functionalization of UiO-66-NH₂ with rhodanine via amidation: towards a robust adsorbent with dual coordination sites for selective capture of Ag(I) from wastewater, *Chem. Eng. J.*, 382 (2020) 123009, doi: 10.1016/j.cej.2019.123009.
- [27] S. Bernt, V. Guillermin, C. Serre, N. Stock, Direct covalent post-synthetic chemical modification of Cr-MIL-101 using nitrating acid, *Chem. Commun.*, 47 (2011) 2838–2840.
- [28] Y. Lin, C. Kong, L. Chen, Direct synthesis of amine-functionalized MIL-101(Cr) nanoparticles and application for CO₂ capture, *RSC Adv.*, 2 (2012) 6417–6419.
- [29] S.Y. Chong, T.T. Wang, L.C. Cheng, H.Y. Lv, M. Ji, Metal-organic framework MIL-101-NH₂-supported acetate-based butylimidazolium ionic liquid as a highly efficient heterogeneous catalyst for the synthesis of 3-Aryl-2-oxazolidinones, *Langmuir*, 35 (2019) 495–503.
- [30] K. Kargosha, N. Shokoufi, J. Azad, Preconcentration and speciation of Sb(III) and Sb(V) with alumina mini column and determination by flame AAS, *Atmos. Spectrosc.*, 28 (2007) 171–177.
- [31] F. Moghimi, A.H. Jafari, H. Yoozbashizadeh, M. Askari, Adsorption behavior of Sb(III) in single and binary Sb(III)-Fe(II) systems on cationic ion exchange resin: adsorption equilibrium, kinetic and thermodynamic aspects, *Trans. Nonferrous Met. Soc. China*, 30 (2020) 236–248.
- [32] P. Ni, R. Zuo, J. Wang, A. Zhou, Adsorption behavior of Sb(III) on iron-functionalized attapulgite in aqueous solution, *Desal. Water Treat.*, 137 (2019) 22–33.
- [33] W. Zhang, R.-Z. Zhang, Y.-Q. Huang, J.-M. Yang, Effect of the synergetic interplay between the electrostatic interactions, size of the dye molecules, and adsorption sites of MIL-101(Cr) on the adsorption of organic dyes from aqueous solutions, *Cryst. Growth Des.*, 18 (2018) 7533–7540.
- [34] X. Li, Y. Mao, K. Leng, G. Ye, Y. Sun, W. Xu, Synthesis of amino-functionalized MIL-101(Cr) with large surface area, *Mater. Lett.*, 197 (2017) 192–195.
- [35] S.-W. Lv, J.-M. Liu, H. Ma, Z.-H. Wang, C.-Y. Li, N. Zhao, S. Wang, Simultaneous adsorption of methyl orange and methylene blue from aqueous solution using amino functionalized Zr-based MOFs, *Microporous Mesoporous Mater.*, 282 (2019) 179–187.
- [36] W. Zhang, R.-Z. Zhang, Y. Yin, J.-M. Yang, Superior selective adsorption of anionic organic dyes by MIL-101 analogs: regulation of adsorption driving forces by free amino groups in pore channels, *J. Mol. Liq.*, 302 (2020) 112616, doi: 10.1016/j.molliq.2020.112616.
- [37] J.M. Park, S.H. Jhung, A remarkable adsorbent for removal of bisphenol S from water: aminated metal-organic framework,

- MIL-101-NH₂, Chem. Eng. J., 396 (2020) 125224, doi: 10.1016/j.cej.2020.125224.
- [38] M.-W. Zhang, K.-Y.A. Lin, C.-F. Huang, S. Tong, Enhanced degradation of toxic azo dye, amaranth, in water using oxone catalyzed by MIL-101-NH₂ under visible light irradiation, Sep. Purif. Technol., 227 (2019) 115632, doi: 10.1016/j.seppur.2019.05.074.
- [39] X. Huang, Q. Hu, L. Gao, Q. Hao, P. Wang, D. Qin, Adsorption characteristics of metal-organic framework MIL-101(Cr) towards sulfamethoxazole and its persulfate oxidation regeneration, RSC Adv., 8 (2018) 27623–27630.
- [40] L.K. Fu, S.X. Wang, G. Lin, L.B. Zhang, Q.M. Liu, H.H. Zhou, C.X. Kang, S.Y. Wan, H.W. Li, S. Wen, Post-modification of UiO-66-NH₂ by resorcylic aldehyde for selective removal of Pb(II) in aqueous media, J. Cleaner Prod., 229 (2019) 470–479.
- [41] J.-Y. Zhang, N. Zhang, L. Zhang, Y. Fang, W. Deng, M. Yu, Z. Wang, L. Li, X. Liu, J. Li, Adsorption of uranyl ions on amine-functionalization of MIL-101(Cr) nanoparticles by a facile coordination-based post-synthetic strategy and X-ray absorption spectroscopy studies, Sci. Rep., 5 (2015) 13514, doi: 10.1038/srep13514.
- [42] Y. Chen, J. Lyu, Y. Wang, T. Chen, Y. Tian, P. Bai, X. Guo, Synthesis, characterization, adsorption, and isotopic separation studies of pyrocatechol-modified MCM-41 for efficient boron removal, Ind. Eng. Chem. Res., 58 (2019) 3282–3292.
- [43] Y.H. Tu, L.F. Ren, Y.X. Lin, J.H. Shao, Y.L. He, X.P. Gao, Z.M. Shen, Adsorption of antimonite and antimonate from aqueous solution using modified polyacrylonitrile with an ultrahigh percentage of amidoxime groups, J. Hazard. Mater., 388 (2020) 121997, doi: 10.1016/j.jhazmat.2019.121997.
- [44] Z. Zhao, X. Wang, C. Zhao, X. Zhu, S. Du, Adsorption and desorption of antimony acetate on sodium montmorillonite, J. Colloid Interface Sci., 345 (2010) 154–159.
- [45] X.Y. He, X.B. Min, X.B.A. Luo, Efficient removal of antimony(III, V) from contaminated water by amino modification of a zirconium metal-organic framework with mechanism study, J. Chem. Eng. Data, 62 (2017) 1519–1529.
- [46] Y. Leng, W. Guo, S. Su, C. Yi, L. Xing, Removal of antimony(III) from aqueous solution by graphene as an adsorbent, Chem. Eng. J., 211 (2012) 406–411.
- [47] Z. Qi, H. Lan, T.P. Joshi, R. Liu, H. Liu, J. Qu, Enhanced oxidative and adsorptive capability towards antimony by copper-doping into magnetite magnetic particles, RSC Adv., 6 (2016) 66990–67001.
- [48] Y. Yan, J.-s. Wang, S.-l. Chen, Y.-x. Bing, Q.-w. Guo, Z.-y. Duan, L. Xie, K.-c. Han, Effective removal of trace antimony(III) from aqueous solution by phosphonic acid-functionalized hollow mesoporous silica spheres as a novel adsorbent, Desal. Water Treat., 174 (2020) 230–239.
- [49] A. Zhou, J. Wang, Removal of antimonite(III) from wastewater using sodium-alginate-modified Fe-attapulgite with sodium alginate beads, Desal. Water Treat., 168 (2019) 282–290.
- [50] N.N. Xiong, P. Wan, G.C. Zhu, F.B. Xie, S.N. Xu, C.Q. Zhu, A.S. Hursthouse, Sb(III) removal from aqueous solution by a novel nano-modified chitosan (NMCS), Sep. Purif. Technol., 236 (2020) 116266, doi: 10.1016/j.seppur.2019.116266.
- [51] J. Zhang, R.-j. Deng, B.-z. Ren, B. Hou, A. Hursthouse, Preparation of a novel Fe₃O₄/HCO composite adsorbent and the mechanism for the removal of antimony(III) from aqueous solution, Sci. Rep., 9 (2019) 13021, doi: 10.1038/s41598-019-49679-9.
- [52] Y. Zou, X. Wang, A. Khan, P. Wang, Y. Liu, A. Alsaedi, T. Hayat, X. Wang, Environmental remediation and application of nanoscale zero-valent iron and its composites for the removal of heavy metal ions: a review, Environ. Sci. Technol., 50 (2016) 7290–7304.
- [53] Z. He, R. Liu, H. Liu, J. Qu, Adsorption of Sb(III) and Sb(V) on freshly prepared ferric hydroxide (FeOxHy), Environ. Eng. Sci., 32 (2015) 95–102.
- [54] H.X. Luo, F.W. Cheng, L. Huelsenbeck, N. Smith, Comparison between conventional solvothermal and aqueous solution-based production of UiO-66-NH₂: life cycle assessment, techno-economic assessment, and implications for CO₂ capture and storage, J. Environ. Chem. Eng., 9 (2021) 105159, doi: 10.1016/j.jece.2021.105159.
- [55] L. Huelsenbeck, H. Luo, P. Verma, J. Dane, R. Ho, E. Beyer, H. Hall, G.M. Geise, G. Giri, Generalized approach for rapid aqueous MOF synthesis by controlling solution pH, Cryst. Growth Des., 20 (2020) 6787–6795.
- [56] C.A. Grande, R. Blom, A. Spjelkavik, V. Moreau, J. Payet, Life-cycle assessment as a tool for eco-design of metal-organic frameworks (MOFs), Sustainable Mater. Technol., 14 (2017) 11–18.